

SITE-DIRECTED SPECTROSCOPIC LABELING OF CARDIAC MYOSIN-BINDING
PROTEIN C FOR INVESTIGATING PROTEIN STRUCTURAL DYNAMICS

By

CHRISTOPHER WANG

A Thesis Submitted to The Honors College

In Partial Fulfillment of the Bachelors Degree

With Honors In

Molecular and Cellular Biology

THE UNIVERSITY OF ARIZONA

MAY 2020

Approved by:

Dr. Brett Colson

College of Medicine

Cellular and Molecular Medicine

ABSTRACT

Cardiac myosin binding protein C (cMyBP-C) is a cardiac muscle protein that serves in the regulation of heart contractility. cMyBP-C mutations can be detrimental to health, promoting cardiac dysfunction and even heart failure. Particularly, abnormal cMyBP-C is associated with hypertrophy of the heart in a genetic condition known as familial hypertrophic cardiomyopathy. Currently, there is no cure for familial hypertrophic cardiomyopathy; treatment for the condition consists only of management of symptoms. Despite cMyBP-C's association with hypertrophic cardiomyopathy, there still exists a void in our knowledge of cMyBP-C dynamics and functions. This is largely because of complexities due to size, disorder, and dynamics that arise when attempting to study it with conventional protein structural biology techniques. Therefore, my project aims to lay the foundation for studying cMyBP-C structure through the use of FRET spectroscopy, a technique that allows the measurement of intramolecular distances at the nanometer scale and structural disorder using fluorescent probe pairs. These probes are introduced at cysteine residues within cMyBP-C using thiol-reactive fluorescent dyes. Using this technique, we have encountered an issue in which our fluorescent dyes are labeling at greater amounts than the number of cysteines endogenous to human cMyBP-C allow for. Therefore, the purpose of this project was to study constructs of cMyBP-C with reduced numbers of endogenous cysteines to seek out the amino acid sites of cMyBP-C being unintentionally labeled, as well as identify improved labeling conditions to minimize observed overlabeling. We concluded that strategic substitution of cysteines with non-cysteine residues dramatically reduced labeling. Overlabeling is also reduced by lowering the pH of the cMyBP-C buffer during labeling. Lastly, FRET probe pairs in cMyBP-C reveal phosphorylation-dependent changes in N-terminal protein structure and dynamics that are important for its regulation of cardiac muscle.

INTRODUCTION

Cardiac Myosin Binding Protein C and its Physiological Significance

cMyBP-C is an isoform of myosin binding protein C that is uniquely present in heart muscle and functions in the regulation of heart contractility (Flashman et al., 2004). cMyBP-C is a myosin-associated protein capable of Protein Kinase A (PKA) mediated phosphorylation, which mediates cMyBP-C's regulatory functions (McNamara et al., 2019). While the precise mechanisms of its role in heart contractility remain unclear, it is cMyBP-C's N-terminal interactions with myosin (thick) and actin (thin) filaments that are of primary interest. cMyBP-C's C-terminus binds to titin and the light meromyosin (LMM) tail of myosin, which anchor it to the thick filament backbone, and also interacts with myosin subfragment 2 (S2) and the myosin regulatory light chain (RLC) at cMyBP-C's N-terminus (Craig et al., 2014). It is of great interest to understand the mechanism of how cMyBP-C dynamically interacts with myosin and actin to contract and relax under various physiological demands, capable of tuning contractility on a beat-to-beat basis.

Heart muscle contraction is induced by interactions between myosin and actin. Myosin and actin produce force as myosin cycles through its chemical-mechanical ATPase cycle that is activated by actin in the presence of ATP to be hydrolyzed. Actin's availability for myosin to bind to it is dependent upon intracellular $[Ca^{2+}]$. The thin filament regulatory complex, troponin-tropomyosin, blocks myosin binding at low $[Ca^{2+}]$ during diastole (filling of heart chambers with blood) and allows for myosin binding at high $[Ca^{2+}]$ during systole (squeezing of blood out of heart to the body). Thus, Ca^{2+} regulates the strength and speed of actin-myosin cross-bridge cycling. cMyBP-C is proposed to function by slowing actin-myosin cross-bridge

cycling kinetics by constraining myosin access to actin through its contacts with the thick filament (Colson et al., 2012; Tong et al., 2008) and/or the thin filament (Shaffer et al., 2009; Luther et al., 2011). An additional function of cMyBP-C interactions with the thin filament may be to activate actin for myosin binding in the absence of Ca^{2+} (Mun et al., 2014). On top of these roles, cMyBP-C itself is regulated by Protein Kinase A (PKA)-mediated phosphorylation to further fine-tune contractile performance.

In the heart, PKA serves to help adjust heart contraction and relaxation dynamics in order to adapt to varying circulatory demands. PKA is activated by stimulation of β -adrenergic receptors (β Rs) by the sympathetic nervous system (SNS). PKA activity targets a number of proteins including cMyBP-C. Phosphorylated cMyBP-C serves to enhance cardiac contractility by accelerating cross-bridge cycling kinetics including cross-bridge formation, force generation, and crossbridge detachment and relaxation by modifying its interactions with thick and thin filaments (Tong et al., 2008; Previs et al., 2016 Robinett et al., 2019). In contrast, when unphosphorylated, cMyBP-C promotes a reserve of myosin heads with lower contractility called the superrelaxed state (SRX) (McNamara et al., 2019). Mutations in cMyBP-C can destabilize SRX (McNamara et al., 2017), causing hypercontractility which has been linked to promotion of the development of heart conditions such as hypertrophic cardiomyopathy (HCM), and ultimately heart failure (Anderson et al., 2018; Kensler et al., 2017). Studies from the Moss laboratory (Stelzer et al., 2006; Tong et al., 2008) have also demonstrated in mouse models that genetic knockout (KO) of cMyBP-C or expression of non-PKA-phosphorylatable cMyBP-C accelerated rates of cross-bridge cycling. These altered interactions between myosin and actin due to the absence of cMyBP-C or its phosphorylation leads to hypertrophy and contractile of the heart tissue. Thus, phosphorylation of cMyBP-C is necessary for normal diastolic function

(Rosas et al., 2015) and heart morphology through critical interactions with myosin and actin in the cardiac sarcomere.

HCM is a disease characterized by diastolic dysfunction and abnormally thickened heart muscle. The impaired relaxation of the heart muscle and increased thickness makes it difficult for the heart to pump blood and can cause symptoms such as shortness of breath, chest pain, fainting, heart palpitations, and heart murmur. In more severe cases, complications such as atrial fibrillation, mitral valve problems, obstructed blood flow, and even heart failure and sudden cardiac death can present (“Hypertrophic cardiomyopathy”, 2018). HCM is most commonly a genetically inherited disease; this subset of HCM is known as familial hypertrophic cardiomyopathy (FHC). FHC is the most common inherited cardiac disease, affecting 0.2%, or 1:500, of the world’s population, and is the leading cause of sudden cardiac death in young adults. In genetically inherited HCM, mutations of cMyBP-C are common. 40% of the associated mutations in inherited HCM are within the gene that encodes for cMyBP-C (Harris et al., 2002; van Dijk et al., 2009). Additionally, HCM is a chronic condition and currently, there is no cure. Treatment focuses primarily on relieving symptoms and preventing sudden cardiac death (“Hypertrophic cardiomyopathy”, 2018). Therefore, study of cMyBP-C molecular structure and its interactions with the heart contractile unit has clinical relevance and can lead to a better understanding of the protein’s function and role in related pathologies such as HCM.

Specifically of interest and this project’s research focus is the N-terminal region of cMyBP-C, consisting of the C0C2 domains (C0C2) of the protein. While the C-terminus of the protein is responsible for anchoring of cMyBP-C to the thick filament backbone, the N-terminus extends away from the thick filament and into the actin-myosin interfilament space, and seems to be able to bind to or interact with the actin filament ((Shaffer et al., 2009; Luther et al., 2011; Mun

et al., 2014). In addition, the N-terminus is also the region that interacts with the S2 and RLC as mentioned previously (Craig et al., 2014). The C0C2 region contains the C0, C1, and C2 domains. It also includes a ~50-residue proline-alanine rich linker (PAL) between C0 and C1, as well as a motif (M) domain between C1 and C2 (Sequeira et al., 2013). Within C0C2 are binding regions capable of interactions with both actin and myosin. The PAL is a flexible region, which allows it to influence the adjacent C0 and C1 domains' interactions with actin and myosin (Colson et al., 2016). Additionally, the M-domain also plays a vital regulatory role. The M-domain itself contains 4 phosphorylatable serine residues that are primarily PKA-phosphorylated, that contribute to regulation of such binding interactions (Gautel et al., 1995, Kensler et al., 2017; Jia et al., 2010). At the level of C0C2, M-domain phosphorylation alters the structural arrangement of the neighboring C1 and C2 molecules as detected by Time-Resolved FRET (TR-FRET) and molecular dynamics computational simulations (Colson et al., 2016). When the same amount (mol/mol) of C0C2 is bound to actin, unphosphorylated C0C2 restricts actin structural dynamics (twisting and bending motions) whereas phosphorylated C0C2 has little effect (Bunch et al., 2019). Thus, at the molecular level (in vitro), phosphorylation alters N-terminal cMyBP-C structure to alter binding to its interaction partners.

Colson et al. (2012) demonstrated the M-domain's regulatory functions in cardiac muscle (in situ) by studying cMyBP-C mutant mice that were rendered either PKA phosphomimetic or non-phosphorylatable by mutating M-domain serine residues. The study used low-angle x-ray diffraction to study the proximity of myosin heads to actin in cardiac muscle fibers. In the phosphomimetic mice, cross-bridges were displaced toward actin, while in non-phosphorylatable mice, molecular mass (myosin head population) was localized closer to the thick filament backbone. Thus, phosphorylation of M-domain in N-terminal cMyBP-C influences interactions

and structure of actin and myosin at the cellular (in situ) and molecular (in vitro) levels to govern contractile function.

Despite this mechanistic knowledge concerning N-terminal cMyBP-C roles in muscle contraction and relaxation, important questions still remain. With the ability to bind a number of different sarcomeric, both thin and thick filament, components, cMyBP-C N-terminal binding effects should be studied further. Under what physiological conditions does C0C2 bind myosin and/or actin in vitro and in situ? How is C0C2 structure altered by PKA phosphorylation dependent binding to myosin and actin? What effects to HCM mutations in C0C2 have on these structure-function relationships? The major focus of my project is develop probes in C0C2 suitable for detecting changes in structure due to phosphorylation, binding, and mutations in vitro, and paving the way for studies in situ. For developing these probes, my project also includes studies of C0C7. While study of truncated N-terminal cMyBP-C is most common, these studies lack the central domains (C3-C7) of cMyBP-C and the C-terminal domains (C8-C10 involved in localization to the sarcomere). These domains are also crucial to understanding cMyBP-C's role in its native physiological location. A recent novel cut and paste technique, developed by the Harris laboratory, has made it possible to study cMyBP-C with probes in the full-length molecule in the cardiac sarcomere. Using Spy-C gene-edited mice, as well as the SpyCatcher-Tag protein ligation system between C7 and C8 domains, genetically encoded C0C7 can be cleaved and recombinant C0C7 can be ligated to C8 and the rest of the thick filament (Napierski et al., 2020). Therefore, Spy-C C0C7 was also used in this project to observe its labeling patterns and set the stage for future in situ studies of N-terminal cMyBP-C structure and function.

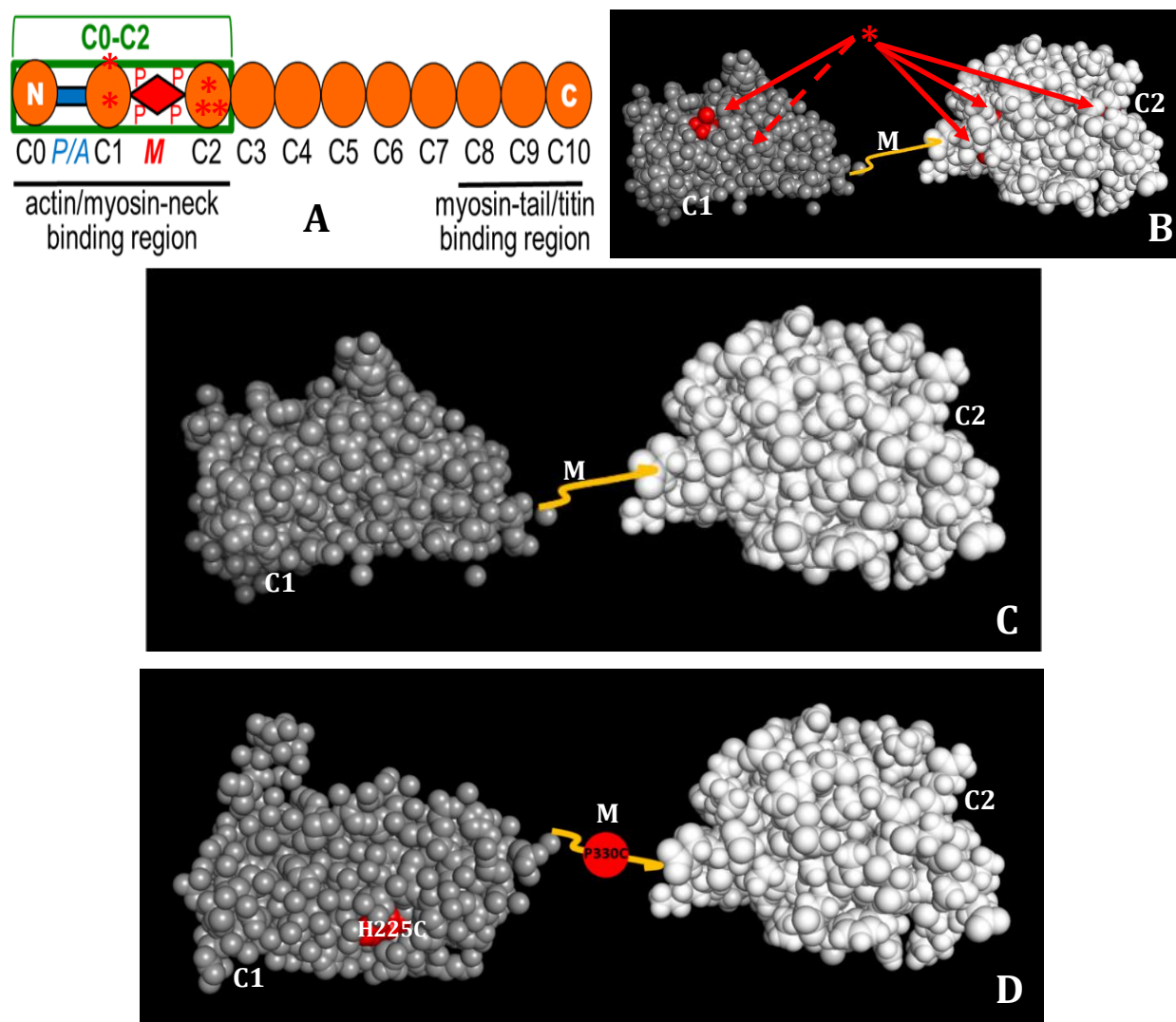


Figure 1. (A) Schematic of cMyBP-C structural organization highlighting the C0-C2 region. The PAL (P/A) and motif (M, with its phosphorylation sites (P)). *Endogenous cysteine residues in the C1-C2 regions (adapted from Colson et al., 2016). (B) Space filling model of C1 (grey) and C2 (white) and motif (yellow) in wildtype C1-C2 and its 5 endogenous cysteines (2 in C1, 3 in C2) highlighted in red. *Cysteine locations, with the dashed line representing a cysteine not currently in view. (C) Space filling model of “ultralite” cMyBP-C, which has had endogenous cysteines substituted out. (D) Space filling model of C1-C2 highlighting the H225C position in C1 and the P330C position in C2) These constructs and positions are described in further detail in *Materials and Methods*.

Current Approach to Studying cMyBP-C Structure, its Complications, and Thesis Objectives

cMyBP-C is a ~150 kDa, ~40 nm long protein with 11 globular domains (C0-C10)(Craig et al., 2014; Finley & Cuperman, 2014). While some atomic images of individual cMyBP-C domains exist, no high-resolution structures of cMyBP-C in its entirety have been captured yet (Finley & Cuperman, 2014; Nag et al., 2017). This is due to a number of reasons. Firstly, the thick filament is a complex, multiprotein entity. Therefore, studying individual components of the thick filament, such as cMyBP-C, is a difficult task to resolve (Nag et al., 2017). In addition, crucial binding and interaction components such as the M-domain and PAL of the C0C2 region are highly dynamic and disordered (Craig et al., 2014). These traits make cMyBP-C difficult to analyze through standard protein structural techniques. However, for the purposes of our studies, we focus on the C0C2 region because of its importance in cMyBP-C's overall regulatory function. Therefore, to study C0C2 structure and interactions, we will utilize site-specific fluorescent labeling for Time-Resolved Fluorescence Resonance Energy Transfer (TR-FRET) measurements of N-terminal cMyBP-C structure and dynamics (Colson et al., 2016). In FRET experiments, two cysteine residue sites in our C0C2 protein are covalently labeled with donor and acceptor site-directed fluorescent probes. Excitation of the donor fluorophore can lead to a dipole-dipole energy transfer from donor to acceptor quencher. This energy transfer can only occur when the donor and acceptor are in close proximity of each other, typically at distances <10 nm (Margineanu et al., 2016; Sekar & Periasamy, 2003). This principle makes FRET an effective technique to use in our research as it allows us to study intramolecular protein structural dynamics between 1-10 nm (keeping in mind cMyBP-C as a whole is ~ 40 nm) with near atomic resolution. FRET is also beneficial in addressing some of the questions regarding C0C2 mentioned in the previous section. In more complex FRET experiments, we are able to probe

C0C2 in various environments, mimicking different physiological states, as well as study C0C2 in the presence of actin or myosin. Additionally, FRET measured in time-resolved mode allows for monitoring of the nanosecond lifetimes of the fluorophores, rather than intensity, which is much less prone to error in the sample preparation, and more importantly, can be analyzed to reveal single molecule-like structural information. This includes resolution of multiple distances between probes attached at specific sites in the protein, quantification of disorder between these sites, and mole fraction of each conformation. These advantages of TR-FRET arise because it effectively allows transient background fluorescence to be ignored, giving more reproducible results (Berthold Technologies GmbH, 2019). In addition, the shape of the fluorescence decay is far richer in structural information than a single data point of fluorescence intensity.

Fluorescence lifetimes are used to calculate FRET efficiency and ultimately, the molecular distances and level of molecular order between probe sites. We also use fluorescent lifetimes rather than fluorescent intensity in TR-FRET because a fluorescent lifetime is an inherent property of a given fluorophore. Lifetimes are relatively independent of fluorophore concentration, absorption by the sample, sample thickness, method of measurement, fluorescence intensity, photo-bleaching, and/or excitation intensity, which again allows for more reliable, and reproducible experiments in comparison to measuring fluorescent intensity (“Fluorescence Lifetime Measurement Advantages & Applications”, n.d.). TR-FRET experiments can therefore be used to provide a greater understanding of cMyBP-C’s dynamic structure (conformations), performed in a variety of physiological conditions. The goal of using TR-FRET experiments is to eventually extend these probes of C0C2 to the full-length molecule and place these molecular rulers in muscle fibers. Another, equally important, avenue stemming from this work is to perform TR-FRET assays on cMyBP-C in the presence of various drug compounds in order to

screen for compounds that reverse hypercontractility in HCM mutants and rescue wildtype cMyBP-C structure, function, and interactions with myosin and actin.

In labeling and intramolecular TR-FRET experiments with human C0C2, we primarily chose fluorescent dyes such as 5-((((2-Iodoacetyl)amino)ethyl)amino)Naphthalene-1-Sulfonic Acid (IAEDANS) and Fluorescein-5-Maleimide (FMAL) as donor labels and N-(4-Dimethylamino-3,5-Dinitrophenyl)Maleimide (DDPM) as an acceptor label. Ideal dyes, such as IAEDANS and FMAL for donor labeling and DDPM for acceptor labeling are relatively small as to not disrupt the host molecule and have substantial overlap (>30%) between donor emission and acceptor absorption spectra, which is quantified by FRET efficiency (E) (Hohng & Ha, 2005; Bajar et al., 2016). These dyes are all also thiol-reactive and should readily react and fluorescently label at sites containing surface exposed cysteine residues. In mouse C0C2, there is 1 surface exposed cysteine compared to 5 total cysteine residues (Colson et al., 2016). Guided by this, we expect a 1:1 dye to protein labeling ratio. However, we have observed a repeated issue in our recent experiments with the human C0C2 constructs having consistent overlabeling by these dyes. This overlabeling persisted even in experiments I have conducted in which mutagenesis was used to produce constructs with a single, or no labelable cysteine residue(s), where I detected fluorescence signaling in constructs that I should not see any response from. We concluded from these experiments that there must be some other non-cysteine site(s) within cMyBP-C that are reactive with our dyes, leading to the observed overlabeling. This overlabeling poses a problem for our lab's work. With consistent overlabeling, we are not able to have full confidence in the results of our labeling and FRET experiments. There is the possibility that FRET is occurring between unintentionally labeled sites on our proteins, or even intermolecularly. Therefore, the overall objectives of this project were to explain the thiol-

reactive dye overlabeling and identify the unknown reactive component, and to test potential solutions to fix or minimize unintentional labeling and maximize intentional cysteine labeling. Resolution of this issue will allow for more confidence, precision, and accuracy in measurements of cMyBP-C intramolecular interactions using FRET spectroscopy

MATERIALS AND METHODS

Terminology and Design of Protein Constructs Used

Several different cMyBP-C protein constructs were used in this project. This study uses the cMyBP-C N-terminal fragment C0C2 and longer fragment C0-C7 (Fig. 1X). The overall plan was to remove and add cysteine residues using site-directed mutagenesis. We tested these constructs for fluorescence dye labeling to determine dye-to-protein ratios and FRET to evaluate cMyBP-C structure by measuring distances between fluorescent dye probes attached to specific cysteines. Here, all relevant constructs are defined and their overall structures are explained:

1. hC0C2_3nHT (WT_C0C2) is the wildtype of cMyBP-C C0C2. Wildtype C0C2 contains 5 total endogenous cysteine residues: 2 in the C1 domain and 3 in the C2 domain (Fig. 1B). There is a 6 histamine tag used for protein isolation on the N-terminal end of the construct. A Tobacco Etch Virus (TEV) cleavage sequence is present after the His tag, allowing the tag to be cleaved off during purification. It should be noted that most C0C2 constructs used in our lab are of the “nHT” (for **N**-terminal **H**is tag and **TEV** cleavage sequence) variant.

2. hC0C2_UL_3nHT (UL_nHT) is an “ultralite” construct of cMyBP-C C0C2 that has had all endogenous exposed cysteines substituted out. This construct is largely used in experiments as a negative control. The ultralite construct is visually represented in Fig. 1C.
3. hC0C2_UL_3cHT (UL_cHT) is akin to the UL_nHT construct, but has the His tag and TEV sequence at the C-terminal of the construct. Like the UL_nHT construct, UL_cHT is also used primarily as a negative control. hC0C2_H225C_3nHT (H225C) is an UL construct with a cysteine substitution at the C1 His225 position in place of an endogenous histamine. This substitution position is visually represented in Fig. 1D.
4. hC0C2_H225C_3nHT (H225C) is an UL construct with a cysteine substitution at the C1 His225 position in place of an endogenous histamine. This substitution position is visually represented in Fig. 1D.
5. hC0C2_P330C_3nHT (P330C) is the same ultralite construct as above, but with a single exposed cysteine substituted in at the Pro330 position (P330C) in the M-domain of C0C2. This substitution position is visually represented in Fig. 1D.
6. hC0C2_H225C,P330C_3nHT (H225C,P330C) is similar to the H225C construct, but with another cysteine substituted in at the Pro330C position. With 2 cysteines engineered in, this is a construct previously discovered by another member of the Colson lab that performs well as a biosensor (Kanassatega, R., personal communication, manuscript in preparation*), meaning that it labels and behaves under FRET spectroscopy appropriately. Specifically, the nanometer distances between FRET probes are sensitive

*manuscript in preparation: R. Kanassatega, T. Bunch, C. Wang, Lepak, and Colson. “A FRET-based biosensor for detecting phosphorylation-dependent structural dynamics in human myosin binding protein-C”

to PKA treatment, which phosphorylates cMyBP-C in the M-domain. This is used throughout the thesis project as a positive control construct.

7. hC0C7_UL_spicy_3nHT (UL_C0C7) is a construct that is ultralite with all cysteines substituted from the beginning C0 through the C7 domain of cMyBP-C.

Construct Design and Validation of Structural Integrity

Sites for potential mutagenesis to generate probe sites and ultralite constructs were found by performing a sequence alignment for C1C2 between a number of MyBP-C isoforms and species. For ultralite constructs, cysteines were preferably substituted for amino acids found in naturally occurring substitutions at the same position in other isoforms and species. This was performed for 4 of the 5 endogenous cysteines in C1C2 (C239L, C249S, C236V, C243S). The last cysteine was widely conserved throughout MyBP-C isoforms and species, and therefore was substituted to a threonine to preserve amino acid chemistry as closely as possible (both are polar, uncharged amino acids). Fig. 2 demonstrates 2 of the ultralite cysteine substitution sites in C2 based on sequence alignment. Substitutions were performed on PyMol computationally before mutagenesis is performed in the wet lab, which predicts the effects of substitutions on cMyBP-C conformation. For all constructs used in this project, no appreciable change in protein conformation or structure was observed. Later, when protein expression had been achieved in BL21-DE3 cells, protein solubility tests using SDS-PAGE gels were conducted, which compares solubility of cMyBP-C protein produced by BL21-DE3 *Escherichia coli* (*E. coli*) grown at various tested temperatures. This allows us to determine the optimal temperature for BL21-DE3 growth to obtain the greatest amount of properly folded, soluble cMyBP-C protein. Solubility

tests for these constructs were performed by other members of the lab, and optimal growth temperature for constructs used in this project was determined to be 23°C, or approximately room temperature. Additionally, circular dichroism (CD) was performed by Rhye Kanassatega on ultralite proteins. Characteristic CDs are imparted by different secondary structural components (α -helices, β -sheets, turns/unstructured regions), allowing CD to act as a predictor of proper protein secondary structure. No significant differences were found between ultralite constructs and wildtype C0C2, meaning that there have been no apparent alterations in C0C2 secondary structure by replacing endogenous cysteines.

```

s-mouse L      T---KYIFEHKGNERIMFINNCSLTDDSEYYVTAGDEKCSSTELFVREPPIMVTKQLEDMN
cX1-danio     S---KYIFESVGNKRFLTINNCSLSDDAAYMCVVGDEKTVTELFVKEPPVLIVRNLEDQM
c-chick       S---KYIFEAIGNKRILTINHCSLADDAAYECVVAEEKSFTTELFVKEPPILITHPLEDQM
c-mus        S---KYIFESVGAKRSLTISQCSLADDAAYQCVVGGEKCSSTELFVKEPPVLITRPLEDQL
c-rab        S---KYIFESVGAKRSLTISQCSLADDAAYQCVVGGEKCSSTELFVKEPPVLITRPLEDQQ
c-hum        S---KYIFESIGAKRSLTISQCSLADDAAYQCVVGGEKCSSTELFVKEPPVLITRPLEDQL
c-dog        S---KYIFESVGAKRSLTISQCSLADDAAYQCVVGGEKCSSTELFVKEPPVLITRPLEDQL
fx1_Danio    A---KYIMEADGNIRTLTINKCSLADDAAYECVVGTDKCFTEVFVKEPPITITKLLDDYH

```

Figure 2. Sequence alignment showing 2 endogenous cysteines in human C2. Highlighted in red is a cysteine that was widely conserved among MyBP-C species and isoforms, which was subsequently substituted for a threonine. The other cysteine, highlighted in green, has naturally occurring substitutions highlighted in blue. In this instance, the cysteine was substituted for a serine, which is present in the same position of chicken. cMyBP-C.

Site-Directed Mutagenesis

Specific primers for each construct were designed on NEBaseChanger. Previously made constructs, carried within a pet45b(+) vector, were used as templates to produce desired plasmid products through high-fidelity PCR using Q5 Hot Start High-Fidelity Master Mix. A 25 μ L PCR reaction was set up on ice with 12.5 μ L of Q5 High Fidelity 2X Master Mix, 1.25 μ L of 10 μ M forward primer, 1.25 μ L of 10 μ M reverse primer, <1,000 ng of template DNA, and nuclease-free water up to 25 μ L. The solution was mixed and then transferred to PCR machine with hot start

lid. PCR thermocycling was performed with temperature parameters guided by the NEB T_m Calculator. PCR product was loaded into an agarose gel and DNA gel electrophoresis was performed to confirm that the desired PCR reaction has taken place.

Confirmation of Plasmid Integration of Construct DNA

PCR product was transformed into NEB5a cell line plates containing Lysogeny broth (LB) and carbenicillin (+carb) to allow for selective growth of NEB5a cells that have successfully incorporated the pet45b(+) plasmids, which contain a carbenicillin resistant gene. Plates were incubated at 37°C overnight to mass-produce the plasmid containing construct DNA. A plasmid miniprep using the ThermoFisher GeneJET Plasmid Miniprep Kit was conducted to isolate plasmids from collected bacteria. First, several NEB5a plate colonies were inoculated in 6 mL of LB+carb and growing at 37°C overnight in an incubator shaker. Bacterial culture was harvested by centrifugation at 6,800 xg in microcentrifuge for 2 minutes. Supernatant was decanted and 250 μ L of resuspension solution was added to the pelleted cells and vortexed. 250 μ L of lysis solution was added and mixed in by inverting tube by hand 4-6 times. 350 μ L of neutralization solution was added and again mixed by inverting tube 4-6 times. The solution was then centrifuged for 5 minutes at >12,000 xg at room temperature. Supernatant was transferred to a GeneJET Spin Column and centrifuged for 1 minute to bind DNA to column. The column was washed by adding 500 μ L of wash solution and centrifuging for 60 seconds at >12,000 xg room temperature. Flow-through was discarded and another wash was repeated. The empty column was centrifuged once more at the same temperature and spin speed. DNA was then eluted by transferring the column to a new tube and adding 50 μ L of nuclease-free water and centrifuging

once more for 1 minute at same temperature and speed. Samples of 8 μL volume and DNA concentration of $\sim 50\text{-}150\text{ ng}/\mu\text{L}$ (concentration determined by NanoDrop spectrophotometer). These samples were sent out to Eton Bioscience for sequencing in order to confirm that the DNA generated from site-directed mutagenesis matches our desired construct sequence. Bacteria from NEB5a colonies that have been confirmed to carry the desired gene were inoculated in LB+carb and grown at 37°C in an incubator shaker overnight and frozen at -80°C for later use.

Protein Expression

Proteins were expressed in the BL21-DE3 cell line. Isolated plasmids were transformed into the BL21-DE3 cells, which are designed to maximize protein production. BL21-DE3 cells were then inoculated onto LB+carb plates and grown at 37°C overnight. Several colonies from each plate were taken and cultured in 2 mL of LB+carb at 37°C for approximately 2 hours, or until the culture was cloudy. This culture was added to 50 mL of LB+carb and incubated 37°C . Growth was monitored every 30 minutes by NanoDrop spectrophotometer OD_{600} reading until OD_{600} of 1 was achieved. Bacterial culture was diluted in 4 L flasks of 500 mL Overnight Express TB+carb media to an initial OD_{600} of 0.04. These large cultures were then shaken and grown at room temperature, or 23°C , overnight until stationary phase is achieved around OD_{600} 4-5, which is confirmed by spectrophotometer. Bacterial culture was collected by centrifugation at 6,000-8,000 $\times g$ for 5 minutes in a JA-10 rotor centrifuge, pouring off of supernatant, and collection of bacterial pellet. The bacterial pellet was resuspended in 25 mL of phosphate-buffered saline (PBS) + 0.1 mM phenylmethylsulfonyl fluoride (PMSF) protease inhibitor. The resuspension was transferred to a 50 mL screw top tube and then centrifuged at 3,300 $\times g$ for 15

minutes. Supernatant was poured off, the weight of pellet was recorded, and the remaining bacterial pellet was frozen at -80°C .

Protein Purification

Bacterial pellets were resuspended in IMAC equilibration buffer (25 mM imidazole, 50 mM Na_2HPO_4 , 200 mM NaCl, 10% glycerol, pH 8) with protease inhibitors (0.1 mM PMSF, EDTA-free protease inhibitor tablet/50 mL) to a volume of 40 mL. Pellets were vortexed until a homogenous solution is achieved. The solution was then passed through an Avastin Emulsiflex C3 homogenizer twice to shear cell walls and lyse cells, releasing cellular contents, including proteins. 1/50 volume 5% polyethyleneimine (PEI) was added and the homogenized solution was centrifuged in a JA-17 rotor for 30 minutes at 17,000 rpm and 4°C , or until supernatant was clear and no longer cloudy to remove insoluble proteins. The lysate, where soluble protein, including cMyBP-C, is localized, was collected.

3 mL of His60 Nickel resin beads (His60 Ni) were equilibrated in IMAC equilibration buffer by centrifugation and washing with buffer 3 times. The collected supernatant was then incubated in the His60 Ni bead suspension for 3 hours to allow for affinity-tagged column chromatography between the His tagged protein and bead column to occur. The beads were then spun down by 2 minute 2,000 rpm centrifugation and batch washed with IMAC equilibration buffer 3-5 times, or until OD_{280} reading of $<0.05-0.07$, to ensure that any undesired protein were washed out of beads. The beads were transferred to a column and washed once more with equilibration buffer until an OD_{280} of $<0.05-0.07$ is confirmed. cMyBP-C protein was eluted from the beads by washing the column with IMAC elution buffer (IMAC equilibration buffer

with 250 mM imidazole added, which outcompetes His tags for bead binding). Elutions were done in 5 mL increments, checking OD₂₈₀ for each elution to determine when protein has been fully eluted. The final concentration of total elution was taken and protein was brought to a concentration of 2 mg/mL, diluted with IMAC elution buffer. 20 µg/mL of Tobacco Etch Virus (TEV) was added to protein solution for TEV cleavage of the His tag, along with 1/1000 volume 0.5 M EDTA and 1 M DTT to allow for proper enzyme reaction. The cleavage reaction was incubated for a 5 hour period at room temperature and then transferred to dialysis tubing and dialyzed against 10X volume of IMAC equilibration buffer minus imidazole (containing 1/1000 volume 0.5 M EDTA and 1 M DTT) overnight at 4°C, to reduce imidazole concentrations to 25 mM. His tags, TEV chains, and uncleaved protein were bound to beads by passing protein solution over 2 mL of His60 Ni beads 5 times over. Isolated cMyBP-C protein, in flow-through, was saved and concentrated to 5-10 mg/mL and dialyzed into a 50 mM NaCl, 50 mM tris buffer, pH 7.5 (50/50).

Fluorescent Labeling of Proteins

Proteins were brought to a concentration of 50 µM in 50/50 buffer. TCEP was added to a concentration of 0.2 mM in solution. The solution was incubated at room temperature for 30 min and aliquoted into light-sensitive tubes in samples of volume between 50-550 µL depending on experiment. These tubes were donor labeled with desired concentrations of IAEDANS or FMAL dye. These labelings were done while gently vortexing the tube and pipetting up and down. Samples were then incubated, covered, on a shaker in the dark for an hour. The samples were

injected into dialysis cassettes and dialyzed 3 times for at least 5 hours each in 100X volume of 50/50 buffer.

A portion of the samples were saved as donor only labeled (DO) samples. The above labeling process was repeated again using desired concentrations of DDPM on the remaining volumes to achieve donor acceptor labeling (DA). The samples were then read on a spectrophotometer wavelength scan between the 250-600 nm light range. Using the known extinction coefficients for IAEDANS ($E_{336\text{nm}} = 5700 \text{ cm}^{-1}\text{M}^{-1}$), FMAL ($E_{473} = 83,000 \text{ cm}^{-1}\text{M}^{-1}$), and DDPM ($E_{440} = 3050 \text{ cm}^{-1}\text{M}^{-1}$) allows us to analyze samples to obtain dye concentration. A BCA assay was performed on these labeled protein samples to determine exact concentrations of cMyBP-C protein in each sample without interference from dye absorbance. Dividing the dye concentration by C0C2 concentration gave us the fraction of C0C2 that was labeled. An SDS-PAGE gel was run with these samples loaded each at a concentration of 2 μg per lane and also at a diluted concentration of .4 μg per lane and imaged for fluorescence via Odyssey CLX to qualitatively observe labeling. The observed labelings were also quantified by measuring the light intensities of fluorescence in these images using Image Studio Lite Software. The gel was stained for 15 minutes with Coomassie Brilliant Blue and then destained with destain buffer (5% MeOH, 7.5% HAc) 3 times for 15 minutes each to observe protein levels and structural integrity. The stained gel was also imaged by Odyssey CLX and analyzed by Image Studio Lite Software. The C1C2 bands were cut out of the gel and sent to Taplin Mass Spectrometry Facility at Harvard where liquid chromatography-tandem mass spectrometry (LC-MS/MS) was performed on the samples to determine which non-cysteine residues were being labeled.

To perform TR-FRET assays on our proteins, a 2x master mix solution was prepared in 50/50 mM NaCl/Tris buffer supplemented with 4 mM MgCl_2 , 0.2 mM ATP, and 0.4 mM DTT.

300 μL of our 2x master mix was combined 1:1 with 10 μM of cMyBP-C protein in 50/50 buffer. From the resulting 600 μL solution, two 280 μL aliquots were prepared for $\pm\text{PKA}$ treatment. For the +PKA samples, PKA was added to a final concentration of 7.5 ng PKA/ μg C0C2 and incubated at 30°C RT for 30 minutes. Following PKA treatment, all samples ($\pm\text{PKA}$) were then aliquoted into a 384-well plate in 50 μL reactions. 5 well repeats of water alone and 5 well repeats of buffer (50/50 buffer with ATP, DTT, and MgCl_2) samples were also included in the multi-well plate in 50 μL s per well. The plate was placed in the TR-FRET instrument (Fluorescence Lifetime Plate Reader, FLTPR). Samples were excited using a passively Q-switched microchip YAG laser at 355 nm with a pulse frequency of 10 kHz and energy of 1 μJ /pulse. Emitted photons were passed through a polarizer set to an angle of 54.7° , then through an interference band-pass filter, and detected with a photomultiplier tube module and digitizer. All FRET experiments were conducted at 25°C. TR-FRET waveforms were analyzed globally. Donor-only labeled C0C2 was best fit to a 3-exponential decay. A single-Gaussian distance distribution was used to fit the FRET data, corresponding to the structural dynamics from C0 to C1 in C0C2 (Colson et al., 2016). Lifetime data was acquired using MatLab Software from the FLTPR instrument for DO $\pm\text{PKA}$ and DA $\pm\text{PKA}$. Average lifetime and standard deviation were calculated for each, accounting for outliers by using a covariance cutoff value of 0.25%. Using average lifetimes, FRET efficiencies (proportion of donor molecules that have transferred excitation state energy to acceptor molecules), and % change of FRET efficiency with PKA treatment were calculated. These values were calculated by Equation 1. and Equation 2. respectively. Equation 3. demonstrates the relationship that FRET efficiency has with distance between donor and acceptor probes. From Equation 3. we can discern that the two have an inverse relationship: as distance between probe sites increases, FRET efficiency decreases.

Equation 4. provides a scoring method through which we are able to assess the quality of our TR-FRET assays (Zhang et al., 1999).

$$E = 1 - \frac{\tau_{DA}}{\tau_{DO}}$$

Equation 1. FRET efficiency (E) calculated using average lifetimes (τ) of DA compared to DO.

$$FRET \% \text{ change} = \frac{E_{+PKA} - E_{-PKA}}{E_{-PKA}}$$

Equation 2. FRET % change is calculated using E of PKA treatment compared to no PKA treatment. This value is only calculated for DA labeling

$$E = \frac{R_0^6}{R_0^6 + R^6}$$

Equation 3. FRET efficiency's (E) relationship to distance between donor and acceptor probes (R). R_0 represents Förster distance between donor and acceptor at which the FRET efficiency is 50%.

$$Z' = 1 - 3\left(\frac{\sigma_A + \sigma_B}{\mu_A - \mu_B}\right)$$

Equation 4. Z' score equation for high-throughput screening (HTS) TR-FRET experiment data analysis. (A) and (B) denote either +PKA or -PKA samples, σ their standard deviations, and μ their means. A score of 0-0.5 indicates good and 0.5-1.0 indicates excellent assay quality (Zhang et al., 1999).

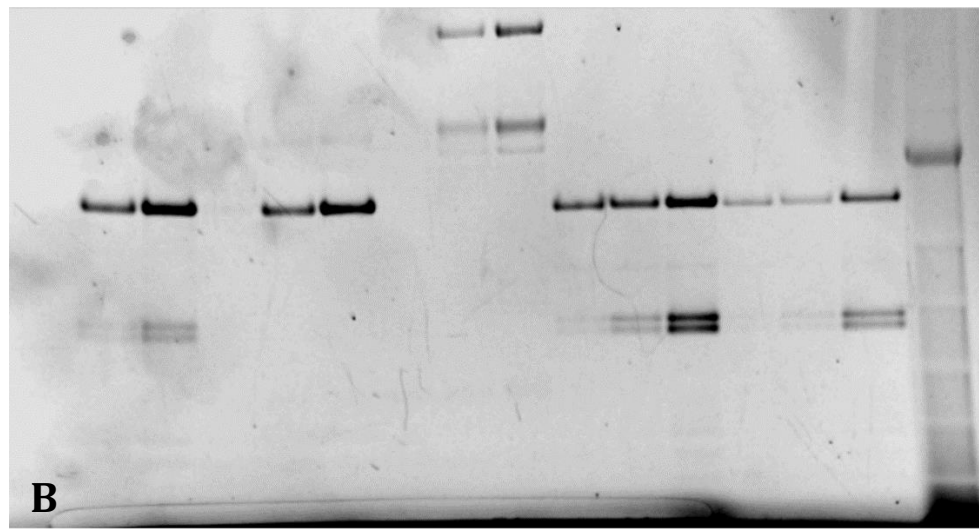
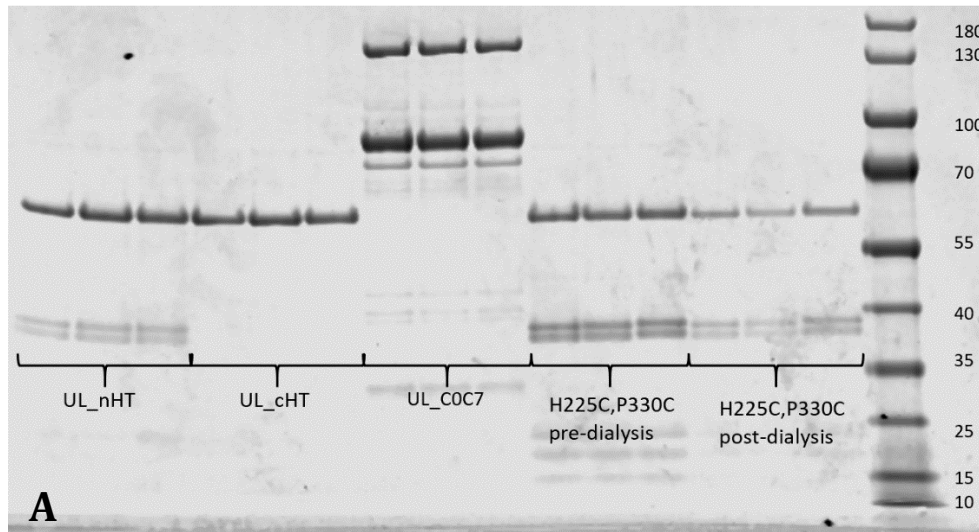
RESULTS

Visualization of Labeling Patterns of cMyBP-C Constructs

A preliminary goal of the project was to visualize labeling trends and patterns across our various cMyBP-C constructs used through gel imaging. UL_nHT, UL_cHT, UL_C0C7, and

H225C,P330C were labeled with 50 μ M, 200 μ M, and 400 μ M of FMAL dye and loaded onto a gel at a concentration of 2 μ g per lane. Imaging of the gel revealed sample loadings and breakdown products, as well as labeling expression through sample fluorescence (Fig. 3A and Fig. 3B). From Coomassie Blue staining, we see no egregious anomalies in protein loading. Loadings across lanes are consistent, allowing comparison of fluorescence in Fig. 3B. For UL_nHT, UL_cHT, and UL_C0C7 samples, there is little to no noticeable fluorescence at the 50 μ M labeled FMAL level. In contrast, the H225C,P330C biosensor demonstrates a distinct labeled band at the 50 μ M FMAL level, even post-dialysis (Fig. 3B). Of our C0C2 samples, fluorescence is also observed in an additional lower band of UL_nHT and H225C,P330C that is not exhibited in UL_cHT (Fig. 3B). This band corresponds to the breakdown product of the N-terminal His tag, suggesting that some component of this His tag byproduct in our protein construct is also being labeled when on the N-terminus as opposed to the C-terminus. Comparing H225C,P330C to UL_nHT, the fluorescence of this nHT breakdown product is observed to be more exaggerated (Fig. 3B). However, this is relatively trivial; Fig. 3A illustrates that the breakdown product has a greater overall presence in the H225C,P330C samples than in UL_nHT, therefore these labelings are proportional. Fluorescence is also observed in the upper bands of the UL_C0C7 construct in the 100 kDa+ range that are not found in any C0C2 constructs (Fig. 3B). In conclusion, Fig. 3 demonstrates that all constructs examined in this experiment, regardless of cysteine content, are capable of being donor labeled by FMAL dye.

In addition to these gels, samples of these protein constructs from the labeling experiment were prepared and sent for LC-MS/MS. However, the results from the LC-MS/MS were inconclusive. The results of the LC-MS/MS indicated low amounts of labeling at many amino acid sites rather than a few unintended sites being predominately labeled.



UL_nHT 50 μ M FMAL
 UL_nHT 200 μ M FMAL
 UL_nHT 400 μ M FMAL
 UL_cHT 50 μ M FMAL
 UL_cHT 200 μ M FMAL
 UL_cHT 400 μ M FMAL
 UL_COC7 50 μ M FMAL
 UL_COC7 200 μ M FMAL
 UL_COC7 400 μ M FMAL
 H225C,P330C pre-dialysis 50 μ M FMAL
 H225C,P330C pre-dialysis 200 μ M FMAL
 H225C,P330C pre-dialysis 400 μ M FMAL
 H225C,P330C post-dialysis 50 μ M FMAL
 H225C,P330C post-dialysis 200 μ M FMAL
 H225C,P330C post-dialysis 400 μ M FMAL
 Protein Ladder

Figure 3. (A) Image of Coomassie Blue stained gel, illustrating sample loadings of FMAL labeled UL_nHT, UL_cHT, UL_COC7, and H225C,P330C. Protein ladder is also depicted to the right with labels corresponding to molecular weights (kDa). (B) Same gel as shown in (A) imaged for fluorescence of FMAL labeled samples of UL_nHT, UL_cHT, UL_COC7, and H225C,P330C.

Quantifications of cMyBP-C Construct Labeling

The same samples from the prior gel experiment were analyzed via spectrophotometric wavelength scan to establish a quantitative estimate of donor cysteine percent (%) labeling for each sample. This % labeling is normalized to the concentration of C0C2 or C0C7 of each sample. This quantification allows comparison with the labeling according to the earlier gel in Fig. 3. An additional labeling experiment with just UL_nHT and H225C,P330C was performed with the same labeling conditions as the first. The results of these experiments are found in Fig. 4 and Fig. 5. respectively.

From the first experiment, I observed that there is labeling above 0% in all constructs at all labeling levels. This labeling is observed even in the ultralite constructs, which have had all cysteine residues substituted out (Fig. 4). Labeling at 50 μ M FMAL was low across all constructs, consistent with our findings from the gel. For the most part, the UL_nHT and UL_cHT constructs behaved similarly outside of the 200 μ M FMAL level; both started at low % labeling and maxed out around 100% at the highest concentrations of FMAL used. The UL_C0C7 construct also labeled similarly, with a slightly lower maximum % labeling, most likely due to its size (Fig. 4). In contrast, the biosensor construct, H225C,P330C, behaved much differently from the other ultralite constructs. It also started at low % labeling, but peaked at around 51% labeling at highest levels (Fig. 4). This is inconsistent with the gel at the 50 μ M FMAL level which shows greater labeling at 50 μ M in comparison to other constructs, but both the gel and labeling percentages suggest that H225C,P330C labeling peaks at lower levels than the other constructs with increasing dye concentration (Fig. 3).

UL_nHT demonstrated similar labeling behavior in the second experiment, peaking at approximately 100% labeling (Fig. 5). In fact, its labeling profile is even more closely related to the UL_cHT and UL_C0C7 constructs from the last experiment, suggesting that all the ultralite constructs labeled in a similar manner. H225C,P330C in this experiment labeled at higher levels than in the prior: its lowest labeling % is equal to its maximum labeling % in the previous experiment and when 200 μ M and 400 μ M FMAL are used, it labels well above 100%. However, it is important to note that these % labeling values are relative to either [C0C2] or [C0C7] and because the H225C,P330C construct contains 2 cysteines per C0C2, it is not overlabeled at any level of FMAL used (Fig. 4 and Fig. 5). In contrast, it is clear that overlabeling is occurring on the other ultralite constructs in this experiment. These constructs contain no cysteine residues, so any labeling at all represents overlabeling within those samples. When saturated with FMAL dye (400 μ M), ultralite labeling seems to peak around 100% (Fig. 4-5). The major conclusion from Figures 4 and 5 is that the labeling observed across all constructs as demonstrated by Fig. 3 is further corroborated. Ultralite constructs are distinctly overlabeled, but di-cysteine H225C,P330C is never overlabeled at any level of FMAL labeling.

The degree of variation in labeling percentages across experiments suggest there are possible variables that I have not yet controlled for. These variables most likely are attributed to the labeling technique itself, which is difficult to reproduce between experiments. Also, of note, because these samples were only donor labeled with FMAL and not intended for use in FRET experiments, BCA assays were not performed to find exact concentration of cMyBP-C protein. I am able to estimate cMyBP-C concentrations closely enough based on the preparation of samples and values via NanoDrop to calculate approximate % labeling, but these are not exact values because dyes can contribute to absorbance at 280-nm and I removed this approximate

contribution. The exact protein concentrations and % labelings are determined before any FRET experiments.

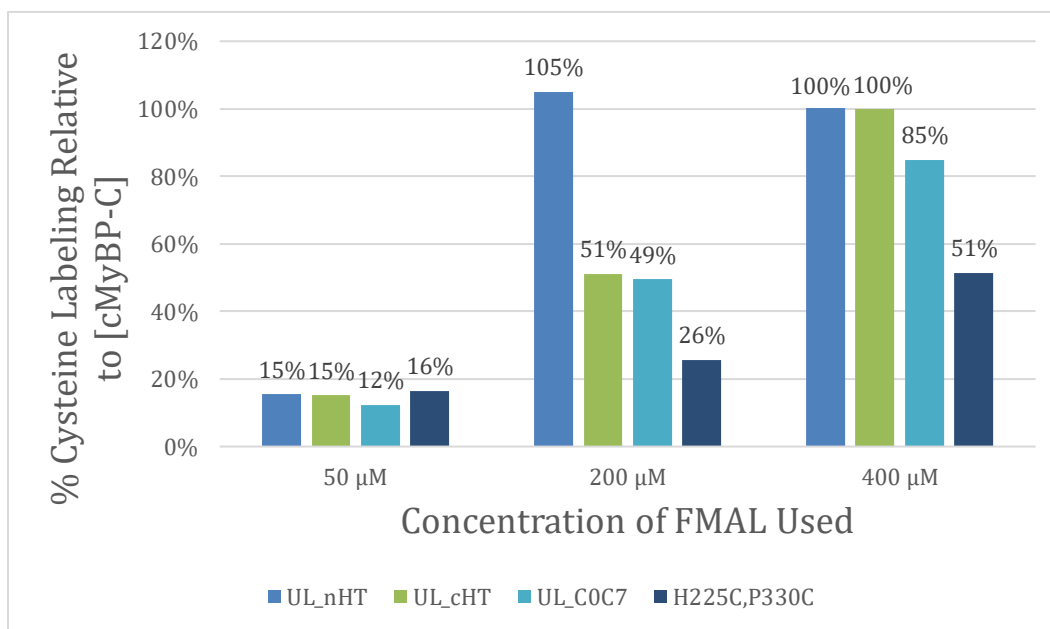


Figure 4. Percent labeling of UL_nHT, UL_cHT, UL_C0C7, and H225C,P330C relative to sample [cMyBP-C] when labeled at 50 μM, 200 μM, 400 μM FMAL as captured by wavelength scan.

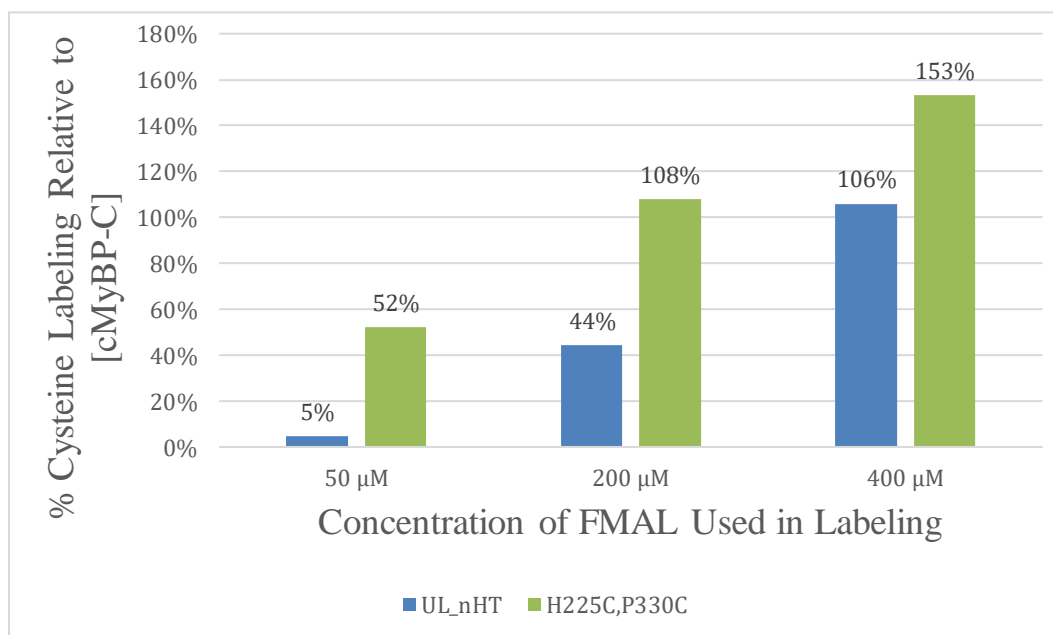


Figure 5. Additional experiment highlighting percent labeling of UL_nHT and H225C,P330C constructs relative to sample [cMyBP-C] when labeled at 50 μM, 200 μM, 400 μM FMAL as captured by wavelength scan.

Varying pH in Labeling of cMyBP-C

The pH of the solution in which cMyBP-C was labeled may influence amount of labeling through manipulation of amino acid chemistry and charges. To test this, I conducted two further labeling experiments with UL_nHT and H225C,P330C with a constant concentration of 200 μ M FMAL in 50/50 buffer (original 50/50 buffer is pH 7.5) at varying pH values (Fig. 6). In addition, I also aimed to test if our buffer solution, which is Tris-based, had any influence in overlabeling. Therefore, I included an additional trial for each cMyBP-C construct at 6.8 pH in phosphate-buffered saline (PBS). The results of this experiment suggest that pH and % labeling are positively correlated. Performing the labelings at pH 8.0 increased % labeling for both constructs in comparison to labeling at 7.5. As labeling pH decreased, so did the extent of labeling. Large changes in the amount of labeling are observed; for instance, there is a 46.61% decrease in labeling from our original pH of 7.5 to 6.5 for UL_nHT (Fig. 6). The decrease in labeling with lowering pH is observed in both UL_nHT and H225C,P330C, but it is important to note that these reductions are not equal given the difference in number of cysteine residues per construct. Labeling percentages for our trials at pH 6.8 in PBS for both constructs fall in trend between trials at pH 6.5 and 8.0, and show no appreciable abnormalities from the other samples in Tris-based buffer (Fig. 6). For following studies in this project, I prepared all buffers and samples at pH 6.5. This seemed to be an optimal pH, as lowering pH further seemed to yield diminishing returns. In addition, we did not want to perturb pH too greatly for the risk of introducing new potential sample issues.

Like the previous experiment, there are apparent differences between % labeling for our constructs and the same pH levels across experiments, suggesting that the aforementioned uncontrolled variables are still influencing our experiments.

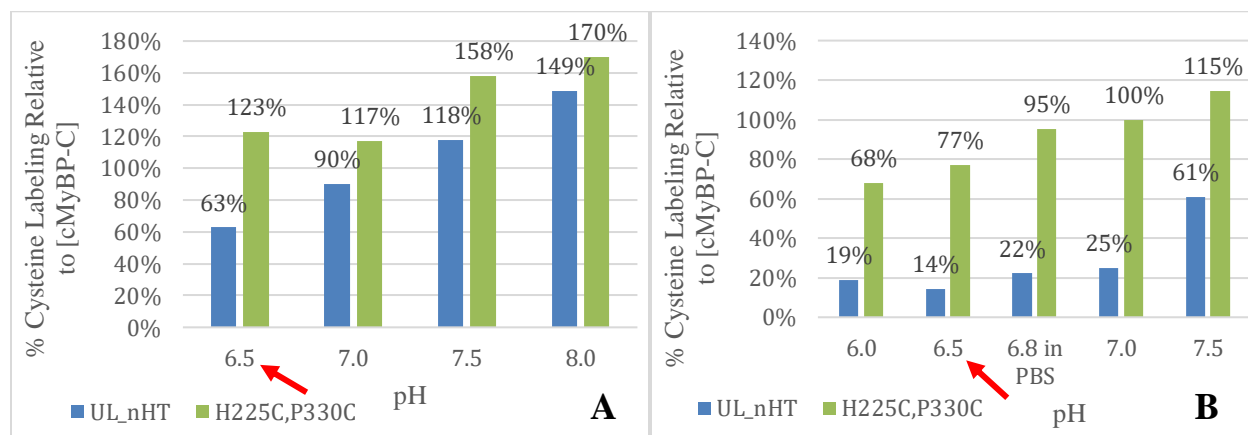


Figure 6. Percentage labeling of cysteines relative to [UL_nHT] and [H225C,P330C] by wavelength scan when prepared at varying pH levels and labeled with 200 μ M FMAL. (A) depicts the first experiment with trials at pH 6.5-8.0 with increments of pH 0.5. (B) depicts additional trials at pH between 6.0-7.5 with increments of pH 0.5 and trial in PBS buffer. Red arrows denote recommended labeling conditions for further experiments.

FRET Experiments With Samples Prepared at pH 6.5

A decrease of buffer pH from 8.0 to 6.5 is a large change on the logarithmic pH scale. Because of this, I wanted to ensure that this change in environmental pH was not impacting protein conformation, and ultimately FRET behavior. To investigate this, I performed labeling experiments at pH 6.5 using P330C, H225C (both single cysteine C0C2 constructs), and H225C,P330C (double cysteine FRET biosensor construct). Each construct was donor labeled with 60 μ M IAEDANS, with a portion saved for donor-only samples (DO). The other portion of sample was further labeled with 300 μ M DDPM to produce DA samples. The results of this FRET experiment, including average lifetimes, FRET efficiencies, % change of FRET, and labeling percentages are highlighted in Table 1. P330C and H225C, which are single-cysteine constructs, are overlabeled according to these labeling parameters, but H225C,P330C (2 cysteines) continues to behave properly, with labeling just slightly over 200% relative to [cMyBP-C] (Table 1.). Therefore, I conclude that at pH 6.5, di-cysteine H225C,P330C still

labels approximately at capacity (relative to cysteine content) while single-cysteine constructs P330C and H225C continue to overlabel even at lower pH. The observed overlabeling despite lowered pH is most likely attributed to the greater ratio of dye to C0C2 concentration used to achieve DA labeling for FRET. Although lower pH proved to decrease % labeling (Fig. 6.), 60 μ M IAEDANS and 300 μ M DDPM were used to label 50 μ M C0C2 protein for FRET (Table 1.), while only 200 μ M FMAL was used to label the same amount of C0C2 protein for the earlier pH experiment (Fig. 6.). Therefore, the greater dye concentration used in FRET studies is thought to counteract the effects of lowering pH. We next tested whether FRET could be observed in the single and double cysteine constructs, and if FRET was sensitive to PKA phosphorylation.

Of emphasis in this data are the FRET efficiency and % change values more so than the lifetimes themselves. We see that P330C exhibits low relative FRET efficiency for both -PKA and +PKA between DO and DA samples (Table 1.). In contrast, the other single cysteine construct, H225C, demonstrates much higher FRET efficiency, even higher than the H225C,P330C biosensor. It is important to note that this value is artificially inflated, as laser intensity had to be increased greatly in order to produce any signal from H225C samples, which is most likely linked to its low levels of DO labeling. It is also important to note that the % change of FRET for both P330C and H225C in this experiment are 0% (Table 1.). FRET efficiency for these constructs remains the same regardless of PKA treatment, indicating no change in FRET behavior. In contrast, the H225C,P330C biosensor also demonstrates an appreciable amount of FRET activity as observed in its FRET efficiency values. However, it exhibits a nonzero % change in FRET of 10%, suggesting that PKA treatment had induced a change in distance between FRET probes (Table 1.), as expected. Based on these results, I

conclude that H225C,P330C is exhibiting FRET activity with two probe sites, but single cysteine constructs are not experiencing any intramolecular FRET even with PKA treatment, as expected. Based on these results, I conclude that there is no intermolecular FRET occurring in single cysteine construct samples, and moreover there is 0% change in FRET with PKA treatment. In contrast, intramolecular FRET is occurring between probe sites on the di-cysteine H225C,P330C construct and this FRET significantly changes upon PKA treatment.

To attempt to control for the variables in labeling affecting earlier experiments, I assisted Rhye Kanassatega in producing a large-scale FRET experiment. The goal of this experiment was to investigate if labeled in the same experiment, whether or not we would be able to observe reproducibility and consistency among samples in FRET data as prepared by two individuals in separate side-by-side labeling experiments. We labeled H225C,P330C with 60 μ M IAEDANS and 200 μ M DDPM. We prepared 255 FRET samples: 15 DO -PKA, 15 DO +PKA, 110 DA -PKA, 115 DA +PKA. FRET efficiency and % change in FRET were calculated based on lifetimes from this experiment (Table 2.). For DO samples of H225C,P330C in this experiment, the % change in lifetimes when untreated and treated with PKA is only -1.15% (Table 2.). Similarly, in the first FRET experiment, the change in lifetimes for H225C,P330C DO \pm PKA is 1.6% (Table 1.). From this, I can conclude that there is little to no difference in lifetimes for DO samples even when treated with PKA. Then, as an indicator of change in FRET due to PKA treatment, we plotted all DA sample lifetimes, including 3 standard deviation bounds (Fig. 7). $\pm 3x$ SD was used to visualize the large difference and small error associated with PKA-sensitive FRET biosensor, whereby the standard deviations do not overlap between -PKA and +PKA groups. This type of analysis (Z' factor) is commonly used in development of high throughput screening (HTS) assays for drug discovery. Again, we observed appreciable FRET activity, with

even greater % change in FRET at 14%, suggesting that the biosensor construct is behaving as intended by detecting large structural effects due to PKA phosphorylation of C0C2 (Table 1.). We also observed that all DA labeled samples fall within 3 standard deviations of the means, demonstrating consistency in labeling, and ultimately FRET. Additionally, no overlap between -PKA and +PKA standard deviation bounds, signaling that there is a significant change in FRET efficiency between PKA untreated and treated samples. Results from an earlier experiment performed by Rhye Kanassatega on H225C,P330C at original pH of 7.5 are also included in for comparison with our large-scale results at pH 6.5 (Table 3.). The labeling parameters of this experiment were 35 μ M IAEDANS and 200 μ M DDPM. FRET efficiency for H225C,P330C is demonstrated within the range of the FRET efficiency displayed in other experiments at pH 6.5, and similar % change in FRET with PKA treatment as well. While the exact labeling numbers fluctuated somewhat between experiments, this can most likely be attributed to the differences in dye concentrations used for labeling. Nevertheless, in all experiments conducted, regardless of pH, H225C,P330C labels almost to max capacity in terms of how many cysteines it contains, but never exceeds this maximum (Table 1-3.).

Table 1. Average lifetimes and their standard deviations, -PKA FRET efficiency, +PKA FRET efficiency, % change in FRET, and labeling % for P330C, H225C, and H225C,P330C labeled at pH 6.5.

Construct	Average Lifetime (ns)	Standard Deviation	FRET Efficiency(E)	% Change FRET	DO % Labeling Relative to [cMyBP-C]	DA % Labeling Relative to [cMyBP-C]
	DO -PKA	11.04	0.15			
	DO +PKA	11.02	0.08			
	DA -PKA	4.44	0.04	60%		
H225C	DA +PKA	4.40	0.10	60%	0%	8%
	DO -PKA	14.38	0.02			
	DO +PKA	14.21	0.02			
	DA -PKA	12.70	0.03	12%		
P330C	DA +PKA	12.55	0.05	12%	0%	67%
	DO -PKA	14.33	0.01			
	DO +PKA	14.10	0.02			
	DA -PKA	9.35	0.02	35%		
H225C,P330C	DA +PKA	9.78	0.01	31%	-12%	61%

Table 2. Average lifetime and its standard deviation, -PKA FRET efficiency, +PKA FRET efficiency, % change in FRET, and labeling % for H225C,P330C in additional large-scale experiment labeled at pH 6.5.

Construct	Average Lifetime (ns)	Standard Deviation	FRET Efficiency(E)	% Change FRET	DO % Labeling Relative to [cMyBP-C]	DA % Labeling Relative to [cMyBP-C]
	DO -PKA	14.70	0.02			
	DO +PKA	14.53	0.02			
	DA -PKA	11.36	0.02	23%		
H225C,P330C	DA +PKA	11.70	0.02	19%	-14%	56%

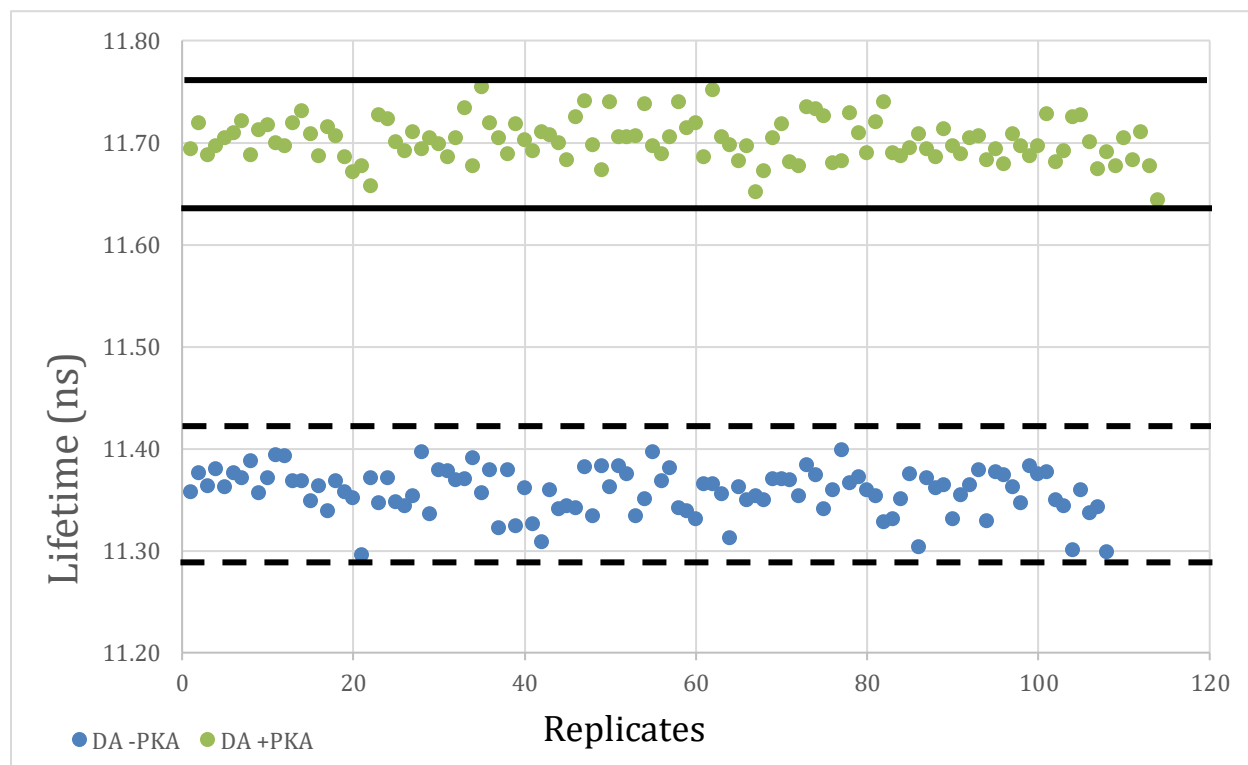


Figure 7. Lifetime data for H225C,P330C DA -PKA and +PKA treatment at pH 6.5 from large-scale experiment shown in Table 2. Lifetimes are plotted in addition to 3 standard deviation bounds for both -PKA (dotted lines) and +PKA (solid lines) separately.

Table 3. Average lifetime and its standard deviation, -PKA FRET efficiency, +PKA FRET efficiency, % change in FRET, and labeling % for H225C,P330C labeled at original pH 7.5.

Construct	Average Lifetime (ns)	Standard Deviation	FRET Efficiency(E)	% Change FRET	DO % Labeling Relative to [cMyBP-C]	DA % Labeling Relative to [cMyBP-C]
DO -PKA	14.70	0.02				
DO +PKA	14.47	0.01				
DA -PKA	10.74	0.01	27%			
H225C,P330C DA +PKA	11.37	0.02	21%	-21%	38%	114%

DISCUSSION

The major objective of this project was to evaluate thiol-reactive labeling of human N-terminal cMyBP-C fragment proteins (C0C2) with zero, one, two cysteines. My goal was to better understand why overlabeling occurs in preparation of C0C2 samples for TR-FRET experimentation. I determined the ratio of dye label to protein under various labeling conditions. We constructed a human cMyBP-C C0C2 "ultralite" construct that has all 5 cysteines substituted out to test for unintended non-specific labeling. We observed much reduced labeling in the ultralite compared to wild type or di-cysteine C0C2. Thus, we can reduce cysteine labeling by removal of endogenous cysteine; however, labeling was not reduced to zero. I also found that lower pH from 7.5 to 6.5 greatly reduced overlabeling of C0C2, whereby very little (negligible) labeling occurred in ultralite constructs lacking cysteines while the C0C2 FRET biosensor with two cysteines was labeled fully. My findings suggest that human C0C2 can be labeled for FRET studies, but that care needs to be taken to ensure that the labeling conditions do not allow for overlabeling of non-cysteine residues.

Overlabeling Occurs Within Ultralite Constructs and Extends to C-Terminal of C0C2

According to SDS-PAGE gel and UV-Vis spectroscopy wavelength scan experiments, overlabeling of ultralite constructs is apparent. Fluorescent bands in protein gels are observed and quantifiable, nonzero percent of labeling for UL_nHT, UL_cHT, and UL_C0C7 was detected, all of which contain no cysteine residues and therefore should not label. All ultralite labeling seems to peak around 100% labeling, or at a 1:1 ratio with [cMyBP-C] (Fig. 3.). This suggests that there is a single non-cysteine component being labeled per molecule of cMyBP-C.

The difference in fluorescence at the 50 μ M FMAL level between ultralite constructs and H225C,P330C suggests that the issue of unexpected labeling in ultralite constructs is largely avoided when utilizing low levels of labeling compounds; overlabeling concerns grow when concentration of dye used is increased (Fig. 3.). Still, this is not very applicable to experimental purposes, as higher concentrations of dye are required to produce suitable labeling of samples for FRET studies. The SDS-PAGE gel also reveals that fluorescent dye is not only found on C0C2, but also the His tag that is engineered on C0C2 constructs for protein purification as demonstrated by the fluorescence of the breakdown product in nHT constructs around the 40 kDa size (Fig. 3.). Thus, non-specific labeling can be reduced by removing the His tag prior to or after labeling.

In contrast to ultralite constructs, H225C,P330C does contain 2 cysteines and did not label past 200% in our quantification experiments even when saturated with labeling dye. I can conclude that overlabeling is a persistent issue in regards to ultralite constructs, but quantifications of biosensor labeling never demonstrate egregious levels of labeling. LC/-MS/MS was unable to reveal exact labeling sites in any cMyBP-C constructs. Because of this, there is no guarantee that H225C,P330C is not being non-specifically labeled at sites outside of its cysteine residues. However, this non-specific labeling is either low or not of concern at all, as demonstrated by the FRET data in this experiment (Table 1-3.). Regardless of exact % labeling or labeling pH, H225C,P330C exhibits consistent FRET activity and corresponding FRET efficiency and % change FRET. This consistency is even displayed in large-scale experimentation with hundreds of samples (Table 2.). This suggests that labeling is contained largely to the two intended cysteine probe sites, which allows H225C,P330C to be used in FRET

studies for its biosensor purposes. Because of this, H225C,P330C is a model construct for FRET experiments.

In the gel, the upper bands of UL_C0C7 correspond to breakdown product of cMyBP-C C-terminal of C0C2. The observed fluorescence in these bands mean that our fluorescent compounds are also labeling to some extent in further sections of cMyBP-C past our emphasis of study. This finding suggests that overlabeling could also pose an issue when performing labeling experiments cMyBP-C beyond the C0C2 domain, and should be kept in mind when conducting future studies of cMyBP-C in greater lengths such as C0C7 or in its entirety (C0C10).

Despite knowing that overlabeling is occurring on ultralite constructs, the LC/-MS/MS was unable to produce any discernible results. Specifically, we were not able to identify a single residue that contained the addition of the dye. We did observe dye attached to many peptides. Thus, the non-specific detection of a labeled peptide suggests that non-specific cysteine labeling is occurring at very low levels at several locations that may vary per labeling experiment. Thus, these experiments will need to be repeated and fine-tuned to identify if there is a single other residue, but our results are so far inconclusive. Nevertheless, the LC-MS/MS can be a powerful tool in identifying specific labeled components of cMyBP-C protein, and so future investigation of these constructs with it may be warranted.

pH of Buffer Influences Labeling: More Acidic Environments Reduce Overlabeling

The pH experiments conducted revealed that by lowering pH, effective labeling percentage was also decreased. This effect is most likely due to the inherent importance pH has in amino acid chemistry. It is possible that decreasing pH impacts the charges on components of

C0C2 that are unintentionally being labeled, rendering them nonreactive with our fluorescent dyes. It is important to note that lowering pH decreased labeling on both ultralite constructs and H225C,P330C. Because ultralite was reduced under the pH 6.5 labeling conditions to near zero, we suspect that the reduction in labeling of H225C,P330C is largely due to this reduction in non-specific labeling.

Additionally, using PBS buffer when preparing samples demonstrated no difference in amount of labeling. Therefore, we can infer that the Tris-based buffer is not promoting overlabeling and that it is appropriate to continue using our standard buffer. Ultimately, we conclude that higher pH can promote overlabeling, which serves as a foundational basis of knowledge to better guide future experiments. Another important note is that because of the disparity between the quantity of cysteines in ultralite and H225C,P330C constructs, reductions in labeling as conveyed through the % labeling in our results are not necessarily equal in regards to concentration of C0C2 cMyBP-C. This logic is involved in deeming pH 6.5 as an appropriate pH for labeling and FRET experiments for the purposes of this study. We observe that between pH 6.5 and pH 6.0, there is no further decrease in labeling for UL_nHT. However, H225C,P330C continues to decrease in labeling %, which is amplified due to the 2 cysteines it contains. Therefore, it was not beneficial to further decrease labeling pH past 6.5. We have established that reducing pH to 6.5 during the labeling procedure, allows for near elimination of labeling in ultralite constructs containing no cysteines, suggesting that labeling of the two cysteine FRET biosensor construct H225C,P330C is labeling only the desired cysteines and not any non-specific residues. These conditions are ideal for intramolecular FRET spectroscopy studies of human C0C2, whereby only the desired cysteine probe sites are labeled to measure intramolecular distances and disorder between the fluorescent donor and acceptor dyes.

FRET Efficiency is Maintained When Lowering pH of cMyBP-C Labeling Buffer

We tested the effect of PKA on C0C2 structure using single cysteine constructs that should not exhibit changes in detected FRET and double cysteine constructs that should exhibit changes in FRET with phosphorylation. The small-scale FRET experiments I performed provided several key results (Table 1.). Despite lowering pH to 6.5, the single cysteine constructs H225C and P330C still experienced overlabeling (Table 1.). However, this overlabeling is most likely attributed to the use of excess acceptor dye in labeling, which may be better tolerated for di-cysteine labeling with 2 cysteines available. Additionally, the P330C probe site seems to label much more readily than the H225C site: P330C demonstrated 67% DO labeling compared to H225C's 8% DO labeling at constant IAEDANS concentration (Table 1.). Could this mean that H225C is experiencing less non-specific labeling? Because of this, in addition to the continued overlabeling observed in both single cysteine constructs, it may be of interest to send H225C and P330C, along with ultralite constructs, for LC-MS/MS to determine which sites are being labeled. Despite overlabeling of H225C and P330C, there is no observed intramolecular FRET for either, which diminishes the concern of overlabeling. From these DO results, we might also expect P330C to be more labeled with donor dye than H225C due to the increased reactivity in the single cysteine samples. Although, FRET with DA labeled samples measures distance between probes and cannot distinguish between which of the two cysteines is labeled with donor versus acceptor. Nevertheless, knowledge of individual site reactivity to labeling is useful for design of future engineered FRET sites in C0C2.

Of note in this experiment was the difficulty in acquiring FRET data for H225C. Compared to the other single-cysteine P330C and di-cysteine H225C,P330C, H225C samples were extremely dim when viewed. This is most likely linked to the poor labeling at the H225C site that was observed (Table 1.). To counteract this and produce a readable signal, the laser intensity of the instrument was amplified for H225C samples. H225C exhibited an uncharacteristically high amount of FRET efficiency, which was probably an artifact due to the higher laser intensity needed to obtain DO and DA lifetimes. Lifetimes of samples with intensity under ~120 mV (without attenuation) are typically unreliable. Because these H225C samples had intensity of only ~ 60 mv, we next looked at whether the observed FRET lifetimes changes with PKA phosphorylation. I observed 0% change of FRET with PKA treatment for both single cysteine constructs, which is reassuring that intermolecular FRET from one C0C2 to another, is not the cause of the change in FRET in the di-cysteine H225C,P330C biosensor. This is consistent with how we expect single cysteine cMyBP-C constructs to behave, as despite conformational changes, there should be no change in FRET because there is only a single probe site.

In contrast, H225C,P330C demonstrates difference in DA FRET efficiency when treated with PKA. This suggests that the conformational changes induced by PKA treatment are reflected by a change in distance between donor and acceptor probe sites on the protein. From this experiment, I can conclude that all 3 constructs are behaving as intended: single cysteine constructs do not reflect change in FRET when treated by PKA while the H225C,P330C biosensor, with 2 cysteine probe sites, does.

Our large-scale FRET experiment also confirms H225C,P330C's efficacy as a biosensor (Table 2. & Fig. 7.). According to this experiment, there is again a substantial % change in FRET

efficiency between untreated and PKA treated DA samples. Additionally, the lifetime, FRET efficiency, and % change FRET values obtained at pH 6.5 are comparable to values obtained with H225C,P330C at pH 7.5. Together with Rhye Kanassatega, we determined that there were no significant changes in PKA induced FRET between labeling at pH 6.5 and pH 7.5. To clarify, these are changes in pH during the labeling procedure. For FRET measurements, all samples were prepared after labeling in buffer at pH 7.5. We were also able to obtain consistent, precise lifetime data through this FRET experiment across a large number of samples produced between 2 different people in separate preparations (Table 2. & Fig. 7.). All H225C,P330C DA -PKA samples and DA +PKA samples are contained within their respective 3x SD bounds. The large-scale FRET experiment with H225C,P330C also demonstrates no overlaps between DA -/+ PKA after 3 SD (Fig. 7). This suggests that PKA treatment is producing a statistically significant change in C0C2 FRET compared to PKA untreated samples.

Using Equation 4. to assess the quality of our large-scale experiment reveals a Z' score of $Z'=0.88$, which indicates that the assay conducted was of excellent quality for use in high-throughput screening (HTS). This Z' score tells us that the cMyBP-C construct used in this project (H2225C,P330C) has sufficient sensitivity for employment in HTS experiments (Zhang et al., 1999). HTS is a powerful analytic method in drug discovery and is discussed the section below in future directions.

Physiological Implications of Findings and Future Directions

We are able to study human C0C2 with constructs that include FRET probes that are able to be labeled with low non-specific labeling. In this project, H225C,P330C represents such a

construct that is able to be used as a FRET biosensor. As discussed in the introduction, cMyBP-C function is heavily regulated via PKA phosphorylation. Thus, in FRET studies with C0C2, which contains the PKA-phosphorylatable region of cMyBP-C, insights to cMyBP-C's conformational dynamics and mechanisms are revealed. In my FRET experiments (Table 1-3.), large changes in H225C,P330C FRET efficiency between untreated and PKA treated samples are observed. When treated with PKA and phosphorylated, FRET efficiency decreases in comparison to H225C,P330C untreated with PKA. FRET efficiency and distance between FRET probe sites are inversely related (Equation 3.), so the observed decrease in H225C,P330C FRET efficiency with PKA treatment suggests that when phosphorylated, the distance between C1 and C2 of cMyBP-C (where our probe sites are located) increases. This conformational change in cMyBP-C serves to alter its interactions to binding partners, further modifying interactions between actin and myosin and ultimately heart contractility. Importantly, this knowledge has much greater physiological and clinical implications. Phosphorylation of cMyBP-C is crucial for normal diastolic function and HCM can arise when mutations in cMyBP-C interfere with its ability to be phosphorylated. Using FRET techniques, studies of human C0C2 can be conducted in many different environments mimicking its native physiological conditions. Z' score analysis on FRET assays of H225C,P330C has demonstrated it to be a viable candidate for further HTS experiments (Equation 4.). Using the H225C,P330C construct, experiments can be conducted comparing untreated DA labeled samples and DA labeled samples treated by various drug compounds, testing C0C2's interactions with many compounds in a single multi-well experiment. A next goal is to identify drug compounds that are able to interact with or bind to C0C2 and mimic phosphorylation, demonstrated by a change in FRET efficiency, and therefore distance between

probe sites, comparable to that of PKA treatment. These compounds would potentially become candidates for further study as potential treatments for HCM.

Future studies with cMyBP-C should also be conducted in greater resemblance of its native physiological state. While experiments with isolated C0C2 are important, much of cMyBP-C, as well as its binding partners, are not present in such experiments. Future FRET studies can be done with C0C2 decorated along with thick and thin filaments in order to determine any influence that these components may have on its structural dynamics. Additionally, exploration utilizing C0C7 SpyC technology (Napierski et al., 2020) will allow us in the future to study phosphorylated cMyBP-C conformational changes past C0C2 and its C-terminal anchoring interactions with the thick filament.

CONCLUSION

Labeling experiments confirmed the occurrence of overlabeling within ultralite constructs, while also validating H225C,P330C's role as a biosensor. We characterized the ultralite zero-cysteine C0C2 construct and determined that while dye labeling was markedly lower than wild type or di-cysteine C0C2, non-specific labeling of non-cysteine residues was still evident. pH was revealed to be an influencing factor in the extent of observed overall labeling; labeling cMyBP-C in more acidic environments appears to limit labeling. While I was not able to determine the specific components of ultralite C0C2 being labeled in this project, this knowledge can be used to minimize the issue of overlabeling. FRET experimentation with cMyBP-C at lower pH revealed that FRET activity, and ultimately cMyBP-C protein dynamics, were preserved even when prepared in a more acidic environment. Despite ultralite and single cysteine

constructs still labeling even at lower pH, their lack of change in FRET efficiency between DA - PKA and DA +PKA trials suggests they are not contributing to the FRET observed in the H225C,P330C FRET biosensor. The 0% change in FRET efficiency for both H225C and P330C suggest that there is no intermolecular FRET between single cysteine molecules of C0C2 occurring within these samples. In contrast, the distinct change in FRET observed in H225CP330C strongly suggests that FRET is occurring between the two probe sites intramolecularly and that this FRET is modified when PKA is introduced (Table 1.). This project has defined the parameters for minimizing non-specific labeling while maximizing intended cysteine labeling of human C0C2 for FRET spectroscopy. My work provides biophysical and mechanistic insight into site-directed labeling and PKA-mediated phosphorylation of human cMyBP-C.

This project provides a solid framework for future studies to be conducted upon. Firstly, the exact details of the overlabeling and non-specific labeling of cMyBP-C still remain unknown. It is particularly interesting that one single cysteine construct (H225C) experiences substantially less labeling than the other construct (P330C). LC-MS/MS analysis was utilized in efforts to specifically determine labeled sites on C0C2, but was ultimately inconclusive. Therefore, LC-MS/MS may be attempted again with ultralite, single-cysteine, and di-cysteine constructs to gain a better understanding of non-specific labeling within C0C2. The discovery of H225C,P330C as a reliable di-cysteine biosensor for FRET experiments introduces the possibility for many more studies. High-throughput screening FRET experiments on C0C2 may be conducted with tens of thousands of drug compounds to screen for compounds that are able to mimic phosphorylation of C0C2. Future studies should also strive to study cMyBP-C beyond C0C2 in isolation. Such studies should similarly aim to first verify that non-specific labeling can be minimized in a way

that it does not interfere with FRET experiments. Possibilities for future FRET experiments will involve studying C0C2 in the presence of cardiac thick and thin filaments.

REFERENCES

- Flashman, E., Redwood, C., Moolman-Smook, J., & Watkins, H. (2004). Cardiac Myosin Binding Protein C. *Circulation Research*, 94(10), 1279–1289.
<https://doi.org/10.1161/01.res.0000127175.21818.c2>
- McNamara, J. W., Singh, R. R., & Sadayappan, S. (2019). Cardiac myosin binding protein-C phosphorylation regulates the super-relaxed state of myosin. *Proceedings of the National Academy of Sciences*, 201821660. <https://doi.org/10.1073/pnas.1821660116>
- Colson, B. A., Thompson, A. R., Espinoza-Fonseca, L. M., & Thomas, D. D. (2016). Site-directed spectroscopy of cardiac myosin-binding protein C reveals effects of phosphorylation on protein structural dynamics. *Proceedings of the National Academy of Sciences*, 113(12), 3233–3238. <https://doi.org/10.1073/pnas.1521281113>
- Anderson, R. L., Trivedi, D. V., Sarkar, S. S., Henze, M., Ma, W., Gong, H., Rogers, C. S., Gorham, J. M., Wong, F. L., Morck, M. M., Seidman, J. G., Ruppel, K. M., Irving, T. C., Cooke, R., Green, E. M., & Spudich, J. A. (2018). Deciphering the super relaxed state of human β -cardiac myosin and the mode of action of mavacamten from myosin molecules to muscle fibers. *Proceedings of the National Academy of Sciences*, 115(35), E8143–E8152. <https://doi.org/10.1073/pnas.1809540115>
- Kensler, R. W., Craig, R., & Moss, R. L. (2017). Phosphorylation of cardiac myosin binding protein C releases myosin heads from the surface of cardiac thick filaments. *Proceedings of the National Academy of Sciences*, 114(8), E1355–E1364.
<https://doi.org/10.1073/pnas.1614020114>

- Harris, S. P., Bartley, C. R., Hacker, T. A., McDonald, K. S., Douglas, P. S., Greaser, M. L., Powers, P. A., & Moss, R. L. (2002). Hypertrophic Cardiomyopathy in Cardiac Myosin Binding Protein-C Knockout Mice. *Circulation Research*, 90(5), 594–601.
<https://doi.org/10.1161/01.res.0000012222.70819.64>
- van Dijk, S. J., Dooijes, D., dos Remedios, C., Michels, M., Lamers, J. M. J., Winegrad, S., Schlossarek, S., Carrier, L., ten Cate, F. J., Stienen, G. J. M., & van der Velden, J. (2009). Cardiac Myosin-Binding Protein C Mutations and Hypertrophic Cardiomyopathy. *Circulation*, 119(11), 1473–1483. <https://doi.org/10.1161/circulationaha.108.838672>
- Sequeira, V., Witjas-Paalberends, E. R., Kuster, D. W. D., & van der Velden, J. (2013). Cardiac myosin-binding protein C: hypertrophic cardiomyopathy mutations and structure–function relationships. *Pflügers Archiv - European Journal of Physiology*, 466(2), 201–206. <https://doi.org/10.1007/s00424-013-1400-3>
- Craig, R., Lee, K. H., Mun, J. Y., Torre, I., & Luther, P. K. (2014). Structure, sarcomeric organization, and thin filament binding of cardiac myosin-binding protein-C. *Pflügers Archiv : European journal of physiology*, 466(3), 425–431.
<https://doi.org/10.1007/s00424-013-1426-6>
- Colson, B. A., Patel, J. R., Chen, P. P., Bekyarova, T., Abdalla, M. I., Tong, C. W., Fitzsimons, D. P., Irving, T. C., & Moss, R. L. (2012). Myosin binding protein-C phosphorylation is the principal mediator of protein kinase A effects on thick filament structure in myocardium. *Journal of molecular and cellular cardiology*, 53(5), 609–616.
<https://doi.org/10.1016/j.yjmcc.2012.07.012>

Tong, C. W., Stelzer, J. E., Greaser, M. L., Powers, P. A., & Moss, R. L. (2008). Acceleration of crossbridge kinetics by protein kinase A phosphorylation of cardiac myosin binding protein C modulates cardiac function. *Circulation research*, 103(9), 974–982.

<https://doi.org/10.1161/CIRCRESAHA.108.177683>

Gautel, M., Zuffardi, O., Freiburg, A., & Labeit, S. (1995). Phosphorylation switches specific for the cardiac isoform of myosin binding protein-C: a modulator of cardiac contraction?. *The EMBO journal*, 14(9), 1952–1960.

Finley, N. L., & Cuperman, T. I. (2014). Cardiac myosin binding protein-C: a structurally dynamic regulator of myocardial contractility. *Pflügers Archiv - European Journal of Physiology*, 466(3), 433–438. <https://doi.org/10.1007/s00424-014-1451-0>

Nag, S., Trivedi, D. V., Sarkar, S. S., Adhikari, A. S., Sunitha, M. S., Sutton, S., Ruppel, K. M., & Spudich, J. A. (2017). The myosin mesa and the basis of hypercontractility caused by hypertrophic cardiomyopathy mutations. *Nature structural & molecular biology*, 24(6), 525–533. <https://doi.org/10.1038/nsmb.3408>

Hohng, S., & Ha, T. (2005). Single-Molecule FRET. In *Molecular Imaging* (pp. 165–179). <https://doi.org/10.1016/b978-019517720-6.50018-3>

Bajar, B. T., Wang, E. S., Zhang, S., Lin, M. Z., & Chu, J. (2016). A Guide to Fluorescent Protein FRET Pairs. *Sensors (Basel, Switzerland)*, 16(9), 1488.

<https://doi.org/10.3390/s16091488>

Hypertrophic cardiomyopathy. (2018, April 14). Retrieved from

<https://www.mayoclinic.org/diseases-conditions/hypertrophic-cardiomyopathy/symptoms-causes/syc-20350198>

Margineanu, A., Chan, J. J., Kelly, D. J., Warren, S. C., Flatters, D., Kumar, S., Katan, M., Dunsby, C. W., & French, P. M. W. (2016). Screening for protein-protein interactions using Förster resonance energy transfer (FRET) and fluorescence lifetime imaging microscopy (FLIM). *Scientific Reports*, 6(1). <https://doi.org/10.1038/srep28186>

Sekar, R. B., & Periasamy, A. (2003). Fluorescence resonance energy transfer (FRET) microscopy imaging of live cell protein localizations. *The Journal of cell biology*, 160(5), 629–633. <https://doi.org/10.1083/jcb.200210140>

Berthold Technologies GmbH. “Time-Resolved FRET (TR-FRET) - Berthold Technologies.” Berthold Technologies GmbH & Co.KG, Berthold Technologies GmbH & Co.KG, 1 Dec. 2019, www.berthold.com/en/bioanalytic/knowledge/glossary/tr-fret/.

“Fluorescence Lifetime Measurement Advantages & Applications.” Sigma Aldrich, www.sigmaaldrich.com/life-science/cell-biology/detection/fluorescence-lifetime-measurement.html.

Napierski, N. C., Granger, K., Langlais, P. R., Moran, H. R., Strom, J., Touma, K., & Harris, S. P. (2020). A Novel “Cut and Paste” Method for In Situ Replacement of cMyBP-C Reveals a New Role for cMyBP-C in the Regulation of Contractile Oscillations. *Circulation Research*, 126(6), 737–749. <https://doi.org/10.1161/circresaha.119.315760>

Shaffer, J. F., Kensler, R. W., & Harris, S. P. (2009). The Myosin-binding Protein C Motif Binds to F-actin in a Phosphorylation-sensitive Manner. *Journal of Biological Chemistry*, 284(18), 12318–12327. <https://doi.org/10.1074/jbc.m808850200>

Luther, P. K., Winkler, H., Taylor, K., Zoghbi, M. E., Craig, R., Padron, R., ... Liu, J. (2011). Direct visualization of myosin-binding protein C bridging myosin and actin filaments in intact muscle. *Proceedings of the National Academy of Sciences*, 108(28), 11423–11428. <https://doi.org/10.1073/pnas.1103216108>

Mun, J. Y., Previs, M. J., Yu, H. Y., Gulick, J., Tobacman, L. S., Beck Previs, S., Robbins, J., Warshaw, D. M., & Craig, R. (2014). Myosin-binding protein C displaces tropomyosin to activate cardiac thin filaments and governs their speed by an independent mechanism. *Proceedings of the National Academy of Sciences*, 111(6), 2170–2175. <https://doi.org/10.1073/pnas.1316001111>

Previs, M. J., Mun, J. Y., Michalek, A. J., Previs, S. B., Gulick, J., Robbins, J., ... Craig, R. (2016). Phosphorylation and calcium antagonistically tune myosin-binding protein C's structure and function. *Proceedings of the National Academy of Sciences*, 113(12), 3239–3244. <https://doi.org/10.1073/pnas.1522236113>

Robinett, J. C., Hanft, L. M., Geist, J., Kontogianni-Konstantopoulos, A., & McDonald, K. S. (2019). Regulation of myofilament force and loaded shortening by skeletal myosin binding protein C. *Journal of General Physiology*, 151(5), 645–659. <https://doi.org/10.1085/jgp.201812200>

McNamara, J. W., Li, A., Lal, S., Bos, J. M., Harris, S. P., van der Velden, J., ... dos Remedios, C. G. (2017). MYBPC3 mutations are associated with a reduced super-relaxed state in patients with hypertrophic cardiomyopathy. *PLOS ONE*, 12(6), e0180064.

<https://doi.org/10.1371/journal.pone.0180064>

Stelzer, J. E., Dunning, S. B., & Moss, R. L. (2006). Ablation of Cardiac Myosin-Binding Protein-C Accelerates Stretch Activation in Murine Skinned Myocardium. *Circulation Research*, 98(9), 1212–1218. <https://doi.org/10.1161/01.res.0000219863.94390.ce>

Rosas, P. C., Liu, Y., Abdalla, M. I., Thomas, C. M., Kidwell, D. T., Dusio, G. F., Mukhopadhyay, D., Kumar, R., Baker, K. M., Mitchell, B. M., Powers, P. A., Fitzsimons, D. P., Patel, B. G., Warren, C. M., Solaro, R. J., Moss, R. L., & Tong, C. W. (2015). Phosphorylation of Cardiac Myosin-Binding Protein-C Is a Critical Mediator of Diastolic Function. *Circulation: Heart Failure*, 8(3), 582–594.

<https://doi.org/10.1161/circheartfailure.114.001550>

Jia, W., Shaffer, J. F., Harris, S. P., & Leary, J. A. (2010). Identification of Novel Protein Kinase A Phosphorylation Sites in the M-domain of Human and Murine Cardiac Myosin Binding Protein-C Using Mass Spectrometry Analysis. *Journal of Proteome Research*, 9(4), 1843–1853. <https://doi.org/10.1021/pr901006h>

Bunch, T. A., Kanassatega, R.-S., Lepak, V. C., & Colson, B. A. (2019). Human cardiac myosin-binding protein C restricts actin structural dynamics in a cooperative and phosphorylation-sensitive manner. *Journal of Biological Chemistry*, 294(44), 16228–16240. <https://doi.org/10.1074/jbc.ra119.009543>

Zhang, J. H., T. D. Chung, and K. R. Oldenburg. (1999). A Simple Statistical Parameter for Use in Evaluation and Validation of High Throughput Screening Assays, *J Biomol Screen*, 4: 67-73.